



RESEARCH ARTICLE



# PUFA-PLs biosynthesis enzymes contribute to pathogenic development of rice blast fungus *Magnaporthe oryzae*

Qiao Liu\*, Ruhui Long\*, Cailing Zhi, Zhibin Liang  and Yi Zhen Deng 

Guangdong Province Key Laboratory of Microbial Signals and Disease Control, Integrative Microbiology Research Centre, College of Plant Protection, South China Agricultural University, Guangzhou, China

## ABSTRACT

Rice blast is one of the most devastating diseases and a serious threat to global food security. It is caused by the ascomycetous fungus *Magnaporthe oryzae*. During the pathogenic development of *M. oryzae*, ferroptotic death of conidial cells is critical for appressorium formation and infection to host rice. In this study, we identified and functionally characterised orthologs of fatty acid desaturase (Fad2) and acyl-CoA synthetase long-chain family (AcsL4) in *M. oryzae*. Pathogenicity was impaired in the *fad2Δ* or *acsl4Δ* mutant and targeted lipidomics analysis demonstrated that Fad2 and AcsL4 were involved in the production of polyunsaturated fatty acids (PUFAs)-containing phospholipids (PUFA-PLs) potentially contributing to ferroptosis. Treatment with FeCl<sub>3</sub>, an oxidative agent to cause lipid peroxidation, could partially restore *fad2Δ* pathogenicity. Fad2 was also found to potentially interact with proteins involved in cellular redox homeostasis. Overall, our results elucidate the role of PUFA-PLs biosynthesis in fungal cell death and fungal pathogenicity, providing a theoretical basis for the development of specific pesticides/drugs targeting ferroptosis caused by lipid peroxidation.

## ARTICLE HISTORY

Received 25 January 2024  
Accepted 26 April 2024



## KEYWORDS

Cell death; ferroptosis;  
*Magnaporthe oryzae*;  
polyunsaturated fatty acids  
(PUFAs); phospholipids  
(PLs); pathogenesis

## 1. Introduction

Rice (*Oryza sativa* L) is a major food crop accounting for up to 50% of the world's total grain production, feeding half of the world's population (Dean et al. 2012; Callaway 2016). However, global food security is threatened by plant diseases (Plant health clinics in Bolivia 2000–2009: operations and preliminary results). Taking rice as an example, loss of rice yield caused by blast disease alone is as high as 10%–30%, annually (Talbot 2003; Yan and Talbot 2016; Fernandez and Orth 2018). Rice blast is a fungal disease that could occur on rice leaves, stalks, ears, and roots (Dufresne and Osbourn 2001; Sesma and Osbourn 2004). The causal pathogen is *Magnaporthe oryzae*, which infects not only rice, but also several other important crops including wheat (*Triticum aestivum*), barley (*Hordeum vulgare*), corn (*Zea mays* L), and millet (*Eleusine corocana*), etc. (Skamnioti and Gurr 2009). Understanding the pathogenic mechanism of *M. oryzae* is of great significance for crop disease management.


During host infection, *M. oryzae* conidia contact the host surface, and then produce the spore-tip mucilage (STM) to adhere closely to the host surface (Hamer et al. 1988). Then the apical cells germinate, and a dome-shaped infection structure termed appressorium is formed on the tip of the germ tube (Dean 1997; Wilson and Talbot 2009; Ryder and Talbot 2015). With the gradual development and maturation of appressorium, substances within conidia are transported to the appressorium, and a large number of macromolecular compounds such as glycerol are produced by substance metabolism (Foster et al. 2017). At this time, a thick layer of melanin is formed inside the appressorium cell wall to prevent the exodus of macromolecules, resulting in a build-up of great turgor pressure (Howard and Valent 1996; Martin-Urdiroz et al. 2016). This mechanical pressure can force penetration of the cuticle of the host surface by penetrating the peg in the ostiole at the base of the appressorium (Howard et al. 1991; Kankanala et al.

**CONTACT** Yi Zhen Deng  [dengyz@scau.edu.cn](mailto:dengyz@scau.edu.cn)  Guangdong Province Key Laboratory of Microbial Signals and Disease Control, Integrative Microbiology Research Centre, College of Plant Protection, South China Agricultural University, Guangzhou 510642, China

\*These authors contributed equally to this work.

This article was originally published with errors, which have now been corrected in the online version. Please see Correction (<http://dx.doi.org/10.1080/21501203.2024.2363655>).

This article has been corrected with minor changes. These changes do not impact the academic content of the article.

 Supplemental data for this article can be accessed online at <https://doi.org/10.1080/21501203.2024.2350169>.

© 2024 The Author(s). Published by Informa UK Limited, trading as Taylor & Francis Group.

This is an Open Access article distributed under the terms of the Creative Commons Attribution-NonCommercial License (<http://creativecommons.org/licenses/by-nc/4.0/>), which permits unrestricted non-commercial use, distribution, and reproduction in any medium, provided the original work is properly cited. The terms on which this article has been published allow the posting of the Accepted Manuscript in a repository by the author(s) or with their consent.

2007; Wilson and Talbot 2009). During appressorium formation and maturation, high levels of endogenous reactive oxygen species (ROS) are generated to strengthen the cell wall (Egan et al. 2007). NADPH (nicotinamide adenine dinucleotide phosphate) oxidase (Nox) can catalyse the generation of substantial quantities of lipid peroxides or ROS, and thus facilitate the rupture of host cells to accelerate pathogen invasion (Egan et al. 2007; Ryder et al. 2013).

Ferroptosis is a type of regulated cell death, depending on the accumulation of intracellular ferric iron ( $\text{Fe}^{3+}$ ) that leads to lipid peroxidation (Dixon et al. 2012; Yang and Stockwell 2016). Ferroptosis has been extensively investigated in animal cells since it was first reported in 2012 (Dixon et al. 2012; Li et al. 2019; Lee et al. 2020; Yang et al. 2023), but research in other organisms has lagged. At present, ferroptosis or ferroptosis-like cell death in plants has only been reported in *Arabidopsis thaliana*, rice, and tobacco (*Nicotiana benthamiana*) cells (Distéfano et al. 2017; Dangol et al. 2019; Macharia et al. 2020). Heat shock (HS) triggers an iron-dependent cell death in *A. thaliana* root cells, which is characteristic of the depletion of GSH and ascorbic acid and the accumulation of cytosolic and lipid ROS (Distéfano et al. 2017). In rice-*M. oryzae* interaction, levels of  $\text{Fe}^{3+}$  and ROS within the plant cells are significantly increased, leading to a ferroptotic death of plant cells as a mechanism of hypersensitive reaction (HR) (Dangol et al. 2019). *N. benthamiana* shows a ferroptosis-like programmed cell death after infection by a highly virulent tobacco mosaic virus mutant (Macharia et al. 2020). Our recent study shows that ferroptosis occurs in the developing conidia of *M. oryzae*, to ensure proper appressorium formation and functioning (Shen et al. 2020). Such ferroptotic death of the developing conidia depends on autophagy function (Veneault-Fourrey et al. 2006), likely by modulating intracellular iron homeostasis (Shen et al. 2020).

PUFAs (polyunsaturated fatty acids) are tend to be oxidised, and the resultant lipid peroxides are capable of damaging the fluidity and permeability of cell membranes and ultimately leading to ferroptotic cell death (Kagan et al. 2017). In plant or animal cells, fatty acid desaturase (Fad2/Fads2) catalyses the formation of a second unsaturated bond of fatty acids, producing PUFAs (Dar et al. 2017; Zhao et al. 2022). In the following step, an enzyme named Acs14 (acyl-CoA synthetase

long-chain family) catalyses the acylation of PUFAs, producing PUFA-CoAs for their subsequent incorporation into phospholipids (PLs), and leading to lipid peroxidation of the cellular membrane (Dai et al. 2023a). It is unclear whether Fad2 and/or Acs14-mediated biosynthesis of PUFA-PLs is involved in fungal cell ferroptosis or pathogenesis. In this study, we characterised the orthologous Fad2 and Acs14 in *M. oryzae*. Both *fad2Δ* and *acs14Δ* mutants were defective in pathogenicity, likely due to compromised conidial death resulting from reduced levels of lipid peroxides during appressorium formation. Lipidomics analysis confirmed that Fad2 and Acs14 were involved in the biosynthesis of PUFA-PLs in *M. oryzae*. Overall, our results reveal that Fad2 and Acs14-mediated PUFA-PLs biosynthesis positively regulates the ferroptosis of developing conidia, which is critical for *M. oryzae* pathogenicity.

## 2. Materials and methods

### 2.1. Growth conditions and strains used in this study

The *M. oryzae* wild-type strain B157 was obtained from Temasek Life Sciences Laboratory, Singapore, and was used in the generation of all transformed/mutants in this study. *M. oryzae* strains were cultivated on Prune agar [PA (1 L), 40 mL prune juice, 2.5 g lactose, 2.5 g sucrose, 1 g yeast extract, 15 g agar, pH 6.5] medium at 25 °C for 3 d in the dark, followed by growth under a 12-h light/12-h dark photoperiod for 4 d to induce conidiation. The colony diameter was measured on PA or complete medium [CM (1 L), 10 g D-glucose, 2 g peptone, 1 g casamino acid, 1 g yeast extract, 0.1% (v/v) trace elements, 0.1% (v/v) vitamin solution, 6 g  $\text{NaNO}_3$ , 1.52 g  $\text{KH}_2\text{PO}_4$ , 0.52 g  $\text{MgSO}_4 \cdot 7 \text{H}_2\text{O}$ , 0.52 g KCl, 15 g Agar, pH 6.5] and the sporulation was quantitatively analysed on PA medium at 10 days. In the stress tolerance assay, the *M. oryzae* mycelial plugs were inoculated on CM medium supplemented with NaCl (0.7 mol/L), KCl (1 mol/L), sorbitol (1 mol/L),  $\text{H}_2\text{O}_2$  (5 mmol/L), SDS (0.01%), or Congo red (CR; 0.2 mg/mL). The fungal cultures were allowed to grow in the dark at 25 °C for 10 days, before recording colony diameter and photo documentation. Mycelial plugs were cultured in liquid CM, at 28 °C, 200 r/min for 2 d before genomic DNA or RNA extraction.

## 2.2. Chemicals used in this study

The following chemicals were used in this study: Trypan blue (Dingguo; AR-0761); C11-BODIPY<sup>581/591</sup> (Thermo FisherScientific; D3861); PE 36:2|18:0\_18:2 (1-stearoyl-2-linoleoyl-sn-glycero-3-phosphoethanolamine; SLPE; Aladdin; 7266-53-7); PE 36:2|18:1\_18:1 (1,2-Dioleoyl-sn-glycero-3-phosphoethanolamine; DOPE; APExBIO Technology; C4956); FeCl<sub>3</sub> (Sigma-Aldrich; 7705-08-0); MEN (menadione; Sigma; 58-27-5); BSO (buthionine sulfoximine; Sigma; B2515); Glu (glutamate; Sigma; 142-47-2). MeOH (0.1%) served as the solvent control for MEN treatment, and EtOH (0.2%) for PEs treatment.

## 2.3. Construction of deletion and complementation plasmids and fungal transformants

Utilising the plasmid pFGL821, which contains the *HPH* hygromycin resistance gene as a vector for gene knock-out, PCR was performed to amplify approximately 1 kb of the regions both upstream and downstream of the *FAD2* and *ACSL4* genes from the genomic DNA of *M. oryzae*, respectively. These upstream and downstream fragments were sequentially cloned into the pFGL821 vector to flank the hygromycin B phosphotransferase cassette (*HPH1*). The resultant *FAD2*-KO or *ACSL4*-KO plasmids were transformed into wild-type strain (B157) via *Agrobacterium tumefaciens*-mediated transformation (ATMT), and deletion of the targeted gene was achieved via homologous recombination. To construct *FAD2*-GFP complementation plasmid, a 3.09 kb DNA fragment (containing 1.27 kb of the *FAD2* native promoter and 1.56 kb of the *FAD2* gene coding sequence without stop codon) was amplified by PCR and then ligated into pFGL1010-GFP. To construct the *ACSL4*-GFP complementation plasmid, DNA fragments of the *ACSL4* native promoter (1.61 kb), the *ACSL4* gene coding sequence without stop codon (2.29 kb), and *eGFP* coding sequence with stop codon (0.7 kb), were amplified by PCR, and sequentially ligated into the pFGL932 plasmid. The resultant plasmids were respectively transformed into *fad2Δ* and *acsl4Δ* mutants by the ATMT method. The sequence of the primers used in this study is listed in Table S1.

## 2.4. Nucleus acid manipulation

*Magnaporthe oryzae* genomic DNA was extracted from vegetative mycelia using E.Z.N.A Fungal DNA Kit (Omega D3390-02). For Southern blotting hybridisation, 5 µg genomic DNA of isolated strains was digested with restriction enzymes, and the products were resolved in a 1% agarose gel and then transferred onto hybond-N1 membrane (Amersham). Specific probes were generated via PCR amplification and subsequently tagged with digoxigenin-11-dUTP by employing the DIG high prime DNA labelling and detection starter kit II from Roche (product number 11585614910). The hybridisation and detection processes were executed following the protocols provided in the instruction manual.

For total RNA extraction, Fastpure® Plant Total Isolation Kit (Vazyme Cat. RC401-01) was used. The synthesis of first-strand cDNA was carried out using the HiScript® III RT SuperMix kit (Vazyme, R323-01).

## 2.5. Staining and microscopic imaging

Conidia were allowed to germinate on Matsunami micro glass slides (Matsunami, Bellingham; S7213) for 6–7 h before C11-BODIPY<sup>581/591</sup> (Thermo FisherScientific; D3861) staining to detect lipid peroxides, following the established protocol (Shen et al. 2020). The confocal microscope (Leica, STELLARIS5, Germany) equipped with an HC PL APO CS2 63×/1.40 oil immersion objective was used for microscopic observation and imaging. Excitation 488 nm and emission 493–581 nm were used for detecting oxidised C11 signals (GFP), *Fad2*-GFP, or *Acsl4*-GFP signals. Excitation 561 nm and emission 581–662 nm were for non-oxidised C11 signals (RFP).

## 2.6. Evaluation of cellular viability

Assessment of conidial death was quantified with conidia (2,000 per droplet, unless otherwise stated) of the *M. oryzae* strain expressing Histone H1-RFP reporter (Shen et al. 2020; Liang et al. 2021) inoculated on hydrophobic coverslips for 14.5 h, using an Axio Observer Z1 microscope (Zeiss, Jena, Germany) equipped with ApoTome.2 camera (Zeiss).

## 2.7. Lipid extraction and comparative lipidomics analysis

Conidia were inoculated on coverslips for 6 h and then harvested for lipid extraction and measurement, following the established protocol (Matyash et al. 2008). At least four independent biological repeats were performed for each instance, each containing  $9 \times 10^6$  conidia.

For comparative lipidomics analysis, 4 biological repeats for each group (WT 6 h, *fad2Δ* 6 h, *acs14Δ* 6 h) were included. Internal standards used in this study include: Octadecanoic-d35 acid (D-2007, as FA 18:0-d35) purchased from C/D/N Isotopes Inc (Pointe-Claire, Quebec, Canada); LPC 18:1-d7 (791643C), LPE 18:1-d7 (791644C), PC 15:0–18:1-d7 (791637C), PE 15:0–18:1-d7 (791638C), PG 15:0–18:1-d7 (791640C), SM d18:1–18:1-d9 (791649C), and TAG 15:0–18:1-d7–15:0 (791648C) purchased from Avanti Polar Lipids (Alabaster, Alabama, USA).

The samples were transferred to 5 mL glass tube, 20  $\mu$ L internal standards (5  $\mu$ g/mL of FA 18:0-d35, PC 15:0–18:1-d7, PE 15:0–18:1-d7, PG 15:0–18:1-d7, and TAG 15:0–18:1-d7–15:0, and 2  $\mu$ g/mL of LPC 18:1-d7, LPE 18:1-d7, and SM d18:1–18:1-d9) and 1 mL MTBE (methyl tert-butyl ether) were added. Followed by vortex, ultrasonication in an ice-water bath for 10 min, and standing at 4 °C for 10 min. Then 800  $\mu$ L supernatant (MTBE phase) was evaporated to dryness. The residues were reconstituted in 50  $\mu$ L dichloromethane/methanol (1:1, v/v) before UHPLC-HRMS/MS analysis. Quality control (QC) sample was pooled from all prepared samples.

Chromatographic separation was executed using a ThermoFisher Ultimate 3000 UHPLC system equipped with a Waters CSH C18 column (2.1 mm  $\times$  100 mm, 1.7  $\mu$ m) at a temperature of 55 °C and a flow rate of 0.3 mL/min. The separation employed mobile phases of (A) water and (B) isopropanol/acetonitrile (9:1, v/v), each containing 10 mmol/L ammonium formate and 0.1% formate for positive mode, and only 10 mmol/L ammonium formate for negative mode. For positive ionisation mode, an injection volume of 1  $\mu$ L was used, following a gradient protocol starting at 40% B for 0 min, increasing to 45% B at 2 min, to 55% B at 4 min where it was maintained until 10 min, reaching 90% B at 14 min, peaking at 95% B by 15 min and held until 18 min, then reverting to 40% B at 18.1 min

and held for 20 min. In contrast, for the negative ionisation mode, the injection volume was adjusted to 3  $\mu$ L while maintaining the equivalent gradient profile and mobile phase composition.

The eluates were subjected to analysis using a ThermoFisher Q Exactive<sup>TM</sup> Hybrid Quadrupole-Orbitrap<sup>TM</sup> Mass Spectrometer (QE), employing Heated Electrospray Ionisation in both Positive (HESI+) and Negative modes (HESI-). The spray voltage for each, HESI+ and HESI-, was maintained at 3.5 kV. Temperatures for both the Capillary and Aux Gas were set at 350 °C, with a sheath gas flow of 40 (Arb) and an Aux gas flow of 10 (Arb). The S-Lens RF level was adjusted to 50 (Arb). The instrument conducted full scans with a resolution of 70,000 FWHM (at m/z 200), covering a mass-to-charge ratio (m/z) range from 130 to 1,950, and an Automatic Gain Control (AGC) Target of  $1 \times 10^6$ . Additionally, fragmentation patterns of the top 10 precursor ions from each scan were captured in a Data-dependent acquisition (DDA) mode using Higher-energy Collisional Dissociation (HCD) at energies of 20, 30, and 40 eV, featuring a resolution of 17,500 FWHM and an AGC Target of  $5 \times 10^5$ .

Structural identification of lipids was performed by LipidMatch (version 3.0.0) (Koelmel et al. 2017), with main parameters as follows, RT Window (for matching peaks to MS/MS scans), 0.14; MZ Search Tolerance MS1 0.005 Da; MZ Search Window MS2, 10 ppm; Intensity Threshold MS2, 1,000.

Initially, UHPLC-HRMS/MS raw datasets were converted into the mzXML format through the use of ProteoWizard software. Following this, the R software platform's XCMS and CAMERA packages were leveraged for data processing. Within the XCMS package, operations such as peak detection [employing the centWave method with parameters: ppm = 5, peak-width = c(5,20), snthresh = 10], chromatographic alignment (bandwidth settings of 6 for the primary grouping and 3 for secondary), and retention time calibration (applying the obiwarp method) were undertaken. The CAMERA package was harnessed to annotate isotopic peaks, adducts, and fragments utilising the predefined settings. Subsequently, a peak table file encapsulating the sample identifiers, retention time, and mass-to-charge (rt mz) variables, and their corresponding peak intensities was produced. The data underwent normalisation by factoring in the internal standards' isotope-labelled peak intensities and the



weight of the samples, setting the stage for further univariate and multivariate statistical analysis.

In the univariate statistical assessment, the data normalisation was carried out using a Student's *t*-test. Potential differential metabolites were marked when the *p* values from the univariate statistical evaluation were less than 0.05 and when there was a fold change (FC) exceeding 1.2. The fold change ( $\text{Log}_2\text{FC}$ ) was determined as the binary logarithm of the mean adjusted peak intensity ratio between Group 1 and Group 2, with a positive value indicating a greater average mass response in Group 1 than in Group 2.

## 2.8. Malondialdehyde (MDA) measurement

Conidia ( $9 \times 10^6$ ) were inoculated on cover slips for 6 h and then harvested for MDA extraction and measurement, using the MDA Assay kit (Suzhou Comin Biotechnology; MDA-1-Y). Three independent biological repeats were performed.

## 2.9. Blast infection assays

For pathogenicity assays, about 14-day-old rice leaves of CO39 were cut and placed in clean Petri dishes, and *M. oryzae* conidial droplets were inoculated onto the detached leaves. The inoculated leaves were kept in the incubator with the setting of high humidity (>90%) and 25 °C, under dark for the first 24 h, and then under dark:light cycle (12 h:12 h). Disease symptoms were examined and photographed at 4–5 d.

## 2.10. Yeast-two-hybrid assay

cDNA library of *M. oryzae* was constructed by Sangon Biotech (<https://www.sangon.com/>), using pGADT7 vector. Bait plasmid (Fad2-BK) was constructed by PCR amplifying *FAD2* CDS from *M. oryzae* cDNA and ligating to pGBKT7 vector. The cDNA library and Fad2-BK were co-transformed to Y2HGOLD Chemically Competent cell (Clontech, YC1002) and then cultured on SD-Trp-Leu medium for 3–5 days at 30 °C. Positive clones were selected and transferred to SD-Trp-Leu-His-Ade medium for further culture at 30 °C for 3–5 days. The positive yeast clones grown on SD-Trp-Leu-His-Ade medium were lysed for plasmid extraction, sequencing, and BLASTN search. Transformation of

pGADT7-T + pGBKT7-53 was used as the positive control, and pGADT7-T + pGBKT7-Lam as negative control.

## 2.11. Statistical analyses

Student's *t*-test was carried out, and *p* values < 0.05 were considered statistically significant.

# 3. Results

## 3.1. Identification of *FAD2* and *ACSL4* genes in *M. oryzae*

To identify *M. oryzae* proteins potentially involved in PUFAs biosynthesis and incorporation to PLs, we used *A. thaliana* Fad2 (Okuley et al. 1994) and *Homo sapiens* Acsl4 (Ding et al. 2023) as the baits to perform BLASTP (<https://blast.ncbi.nlm.nih.gov/Blast.cgi>) search. The orthologous enzymes were identified, namely Fad2 (XP\_003708723.1) and Acsl4 (XP\_003714525.1). Fad2 encoded by *MGG\_01985* belongs to the Membrane-FADS-like superfamily (Figure S1A). Acsl4 encoded by *MGG\_01551* belongs to AFD\_class\_I superfamily (Figure S1B). Phylogenetic analysis shows that *M. oryzae* Fad2 and Acsl4 are conserved within filamentous fungi, closely related to *Gaeumannomyces tritici* and *Magnaporthe oryzae* Fad2 (XP\_009226527.1 and KLU92396.1) and Acsl1 (XP\_009220132.1 and KLU81404.1), respectively (Figure S1A–B). *Magnaporthe oryzae* Fad2 and Acsl4 are evolutionarily distant from Fad2/Fads2 and Acsl4 orthologs in plants or animals, which form distinct clades from the fungal clades (Figure S1A–B).

## 3.2. Biological function of *FAD2* and *ACSL4* genes

To investigate the functions of *M. oryzae* *FAD2* and *ACSL4* genes, we deleted these genes individually in the wild-type (WT, B157) background by homologous recombination strategy (Figure S2A–B). The *fad2Δ* and *acsl4Δ* mutants were verified by Southern blotting (Figure S2C–D). Genetic complementation of the *FAD2* or *ACSL4* gene in the respective mutant was verified by PCR and RT-qPCR analysis (Figure S2E–F).

The *fad2Δ* mutants showed an obvious decrease in mycelial colony diameter when grown on CM medium, which was restored in the complementation

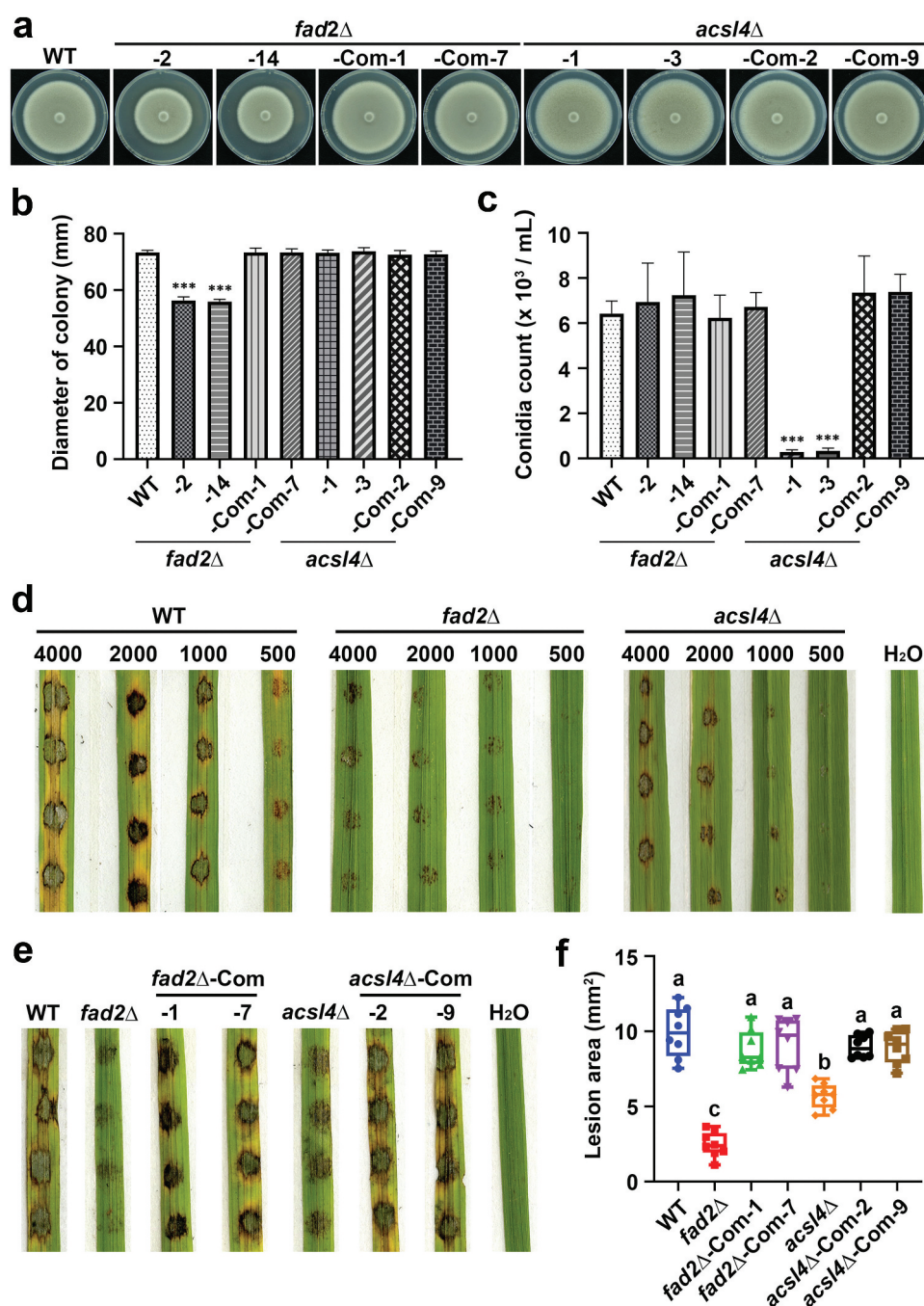


**Figure 1.** *FAD2* and *ACSL4* are involved in mycelial growth, conidiation, and pathogenicity in *Magnaporthe oryzae*. (a) Colony morphology of the wild-type strain (WT), *fad2* $\Delta$  mutants, *fad2* $\Delta$ -Com, *acsl4* $\Delta$  mutants, and *acsl4* $\Delta$ -Com strains grown on CM (complete medium). Photographs were taken at 10 d post-inoculation. (b) Quantification of the diameter of the colonies grown on CM. Barchart depicting quantification (mean  $\pm$  S.D.) was derived from three independent repeats for each treatment. \*\*\*:  $p < 0.001$  vs WT (Student's *t*-test). (c) Quantification of conidiation production in WT, *fad2* $\Delta$  mutants, *fad2* $\Delta$ -Com, *acsl4* $\Delta$  mutants, and *acsl4* $\Delta$ -Com strains, mean  $\pm$  S.D. was derived from three independent biological repeats. \*\*\*:  $p < 0.001$  vs WT (Student's *t*-test). (d) Conidial suspension of different inoculums (4,000, 2,000, 1,000, or 500 conidia/droplets) from WT, *fad2* $\Delta$ , or *acsl4* $\Delta$  mutants were placed on rice leaf explants. The inoculated leaves were kept under constant dark conditions for 24 h and then moved to a growth chamber with the setting of cyclic dark:light condition (12 h:12 h). Disease symptom was assessed and photographed at 5 d post-infection. (e) Infection assay with WT, *fad2* $\Delta$ , *acsl4* $\Delta$ , *fad2* $\Delta$ -Com, and *acsl4* $\Delta$ -Com strains. Same procedure as in (d). The conidia inoculum for each strain was 2,000 conidia/droplet. (f) Box plots depicting lesion area caused by conidia of WT, deletion, or complementation strain. At least two independent biological repeats were performed for each instance,  $n = 8$ . Different letters denote significant differences ( $p < 0.05$ ).

strain (Figure 1a–b). On the other hand, conidia production was significantly reduced in *acsl4*Δ, but not in *fad2*Δ, compared to WT (Figure 1c). Genetic complementation of the *ACSL4* gene could fully restore such conidiation defect (Figure 1c). Next, we evaluated the role of Fad2 and Acsl4 in fungal pathogenicity, by inoculating serial diluted conidial droplets (each containing 4,000, 2,000, 1,000, or 500 conidia, respectively) on detached rice leaves. The *fad2*Δ or *acsl4*Δ conidia caused reduced blast lesions as compared to WT conidia, and such pathogenicity defects were likely cell-density dependent (Figure 1d). Genetic complementation of *FAD2* or *ACSL4* gene could fully restore such pathogenicity defect of the respective mutant (Figure 1e–f), confirming that Fad2 and Acsl4 are indeed required for *M. oryzae* pathogenicity.

To further investigate the potential mechanism of Fad2 or Acsl4 in regulating *M. oryzae* pathogenicity, we then evaluated the appressorium formation rate (%) in the mutants in comparison to WT. We found that the appressorium formation rate was remarkably reduced in the *fad2*Δ mutant at an early stage (6 or 12-h post-inoculation, hpi) while caught up to a level comparable to WT, in the later stage (24 hpi; Figure 2a). The appressorium formation rate of the *FAD2*-Complementation strain (*fad2*Δ-Com) was comparable to that of the wild type (Figure 2a). On the other hand, no significant difference in appressorium formation rate in the *acsl4*Δ compared to WT or *acsl4*Δ-Com conidia, as early as 6 hpi on the inductive surface (Figure 2b). We conclude that loss of *FAD2* led to a delay in appressorium formation. To investigate whether pressure turgor generation within the mature appressorium was affected in the *fad2*Δ or *acsl4*Δ mutant, we assessed the collapse rate (%) of appressoria under treatment of exogenous glycerol. The results showed that there was no significant difference in the *fad2*Δ or *acsl4*Δ mutants compared to WT or their respective complementation strains (Figure 2c). We further examined the rate (%) of infection hyphae (IH) grown on barley leaves at 24 and 48 hpi respectively. The result showed that at 24 hpi, the percentage of type 1 (no IH) formed by *fad2*Δ or *acsl4*Δ appressoria was close to 70%, while was around 40% in WT (Figure 2d). In contrast, the sum

of type 2 and 3 appressorium (with IH in the directly infected host cell) formed by WT appressoria was 60% while less than 30% in *fad2*Δ or *acsl4*Δ (Figure 2d). At 48 hpi, around 50% of WT appressoria formed type 4 IH (spread to the neighbouring host cells) while that of *fad2*Δ or *acsl4*Δ was less than 20% (Figure 2d). Such delayed/lagged invasive hyphae growth phenotype could be fully restored by genetic complementation of *FAD2* or *ACSL4* gene respectively (Figure 2d). This result demonstrates that Fad2 and Acsl4 are important for invasive growth during host infection.

Overall, our results demonstrate that Fad2 and Acsl4 are both involved in mycelial growth and pathogenicity, and Acsl4 is also important for conidiation.

### 3.3. *Fad2 and Acsl4 regulate conidial death in M. oryzae*

We next assessed whether conidial cell death was affected in the *fad2*Δ or *acsl4*Δ mutant, during appressorium formation. Consistent as reported (Shen et al. 2020), sequential cell death occurred at 7–15 hpi, usually starting from the distal cell of the germ tube and the nascent appressorium, and spread towards the proximal cell, which could be visualised by the dynamics of H1-RFP marked nuclei (Figure 3a). At 14.5 hpi on the inductive surface, we quantified conidial viability (including conidial cells all survived and 1–2 conidial cells survived as illustrated in Figure 3a) based on H1-RFP marked nuclei in conidia of wild-type, mutant, or complementation strain. We noticed that the *fad2*Δ or *acsl4*Δ mutants displayed higher cell viability (%) compared to the wild type (Figure 3b–c). Such defect in conidial cell death could be fully restored by genetic complementation of *FAD2* or *ACSL4* genes (Figure 3b–c). These results reveal that Fad2 and Acsl4 are required for timely conidial death.

We further assessed whether accumulation of lipid peroxides, a prerequisite for conidial cell death, was affected in developing conidia of *fad2*Δ or *acsl4*Δ. The fluorescent dye C11-BODIPY<sup>581/591</sup> (Drummen et al. 2002; Carlsen et al. 2009; Dai et al. 2023b) was used to stain the WT or mutant conidia at 6 hpi. The oxidised C11-BODIPY<sup>581/591</sup> signal (green fluorescence) was much



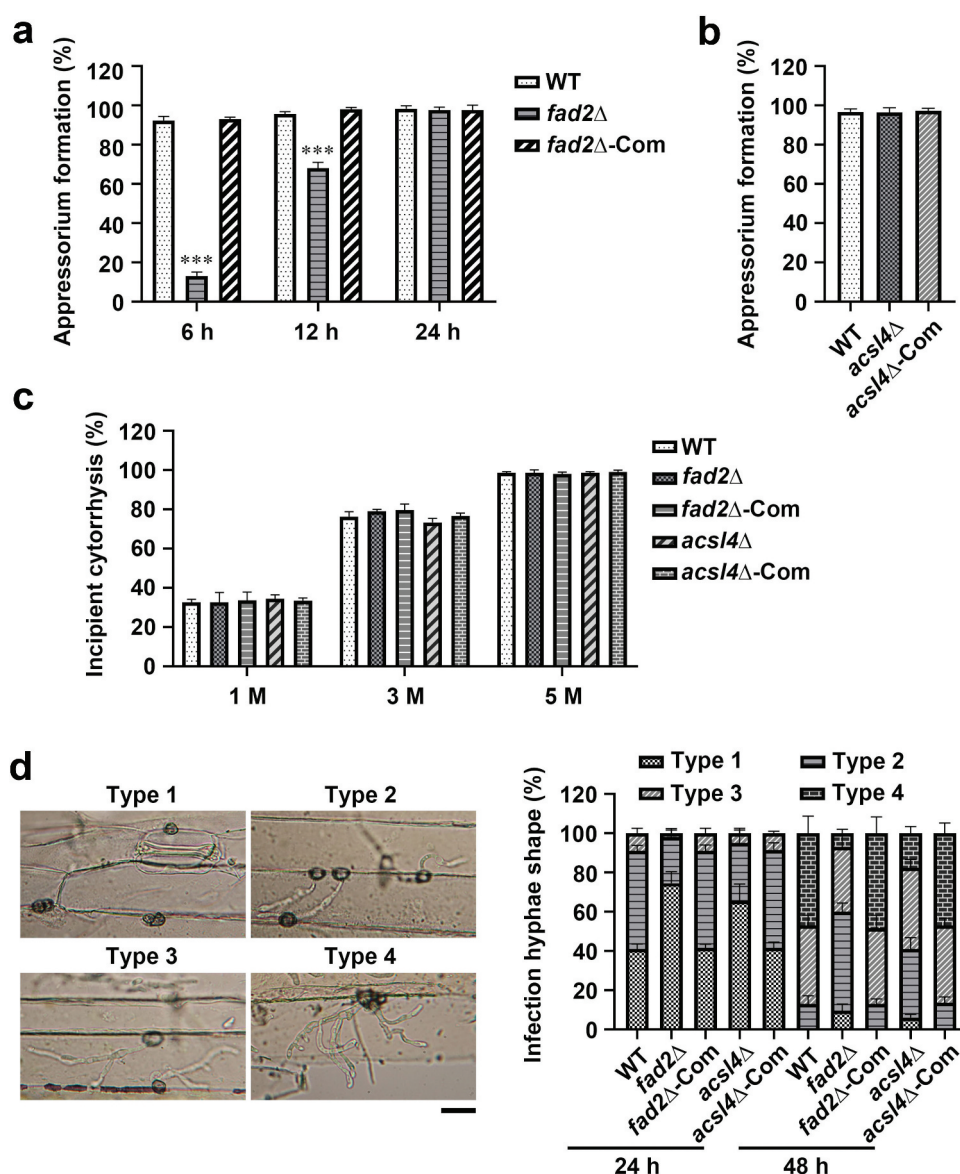


**Figure 2.** Assessment of appressorium formation, turgor generation, and mycelial hydrophobicity. (a) Quantification of appressorium formation rates (%) of WT, *fad2*Δ, or *fad2*Δ-Com at 6, 12, or 24 h post-inoculation (hpi) on the inductive surface (hydrophobic surface). Mean  $\pm$  S.D. was derived from three independent biological repeats. \*\*\*:  $p < 0.001$  vs WT at 6 or 12 h, respectively. (b) Quantification of appressorium formation rates (%) of WT *acs14* mutant or *acs14*Δ-Com at 6 hpi. Mean  $\pm$  S.D. was derived from three independent biological repeats. (c) Quantification of appressorium collapse rates (%) in WT, *fad2*Δ, *fad2*Δ-Com, *acs14*Δ, or *acs14*Δ-Com at 24 hpi, under treatment with 1, 3, or 5 mol/L glycerol solutions for 3 min. Mean  $\pm$  S.D. was derived from three independent repeats for each treatment. (d) Different stages of invasive growth (types 1–4) inside the barley leaf inoculated with WT, *fad2*Δ, *fad2*Δ-Com, *acs14*Δ, or *acs14*Δ-Com conidia (2,000 conidia/droplet). Scale bar = 10  $\mu$ m. Quantification of invasive hypha rate ( $n = 50$ ) was derived from three independent biological repeats. Type 1: No invasive hyphae; type 2: Invasive hyphae no branching; type 3: Invasive hyphae with more than 1 branch within one host cell; type 4: Invasive hyphae has spread to adjacent cells.

lower in the *fad2*Δ or *acs14*Δ conidia than that in WT, but of a comparable level in the genetic complementation strains to WT (Figure 4a). Quantitative analysis of the mean fluorescence intensity (MFI) ratio of green/total fluorescence was performed following the established

methods (Jofre-Monseny et al. 2007; Taylor et al. 2013; Wang et al. 2023), confirming that lipid peroxidation was reduced in the *fad2*Δ and *acs14*Δ conidia (Figure 4b). The level of intracellular malondialdehyde (MDA) is also used to reflect the level of lipid peroxidation (Gaschler and



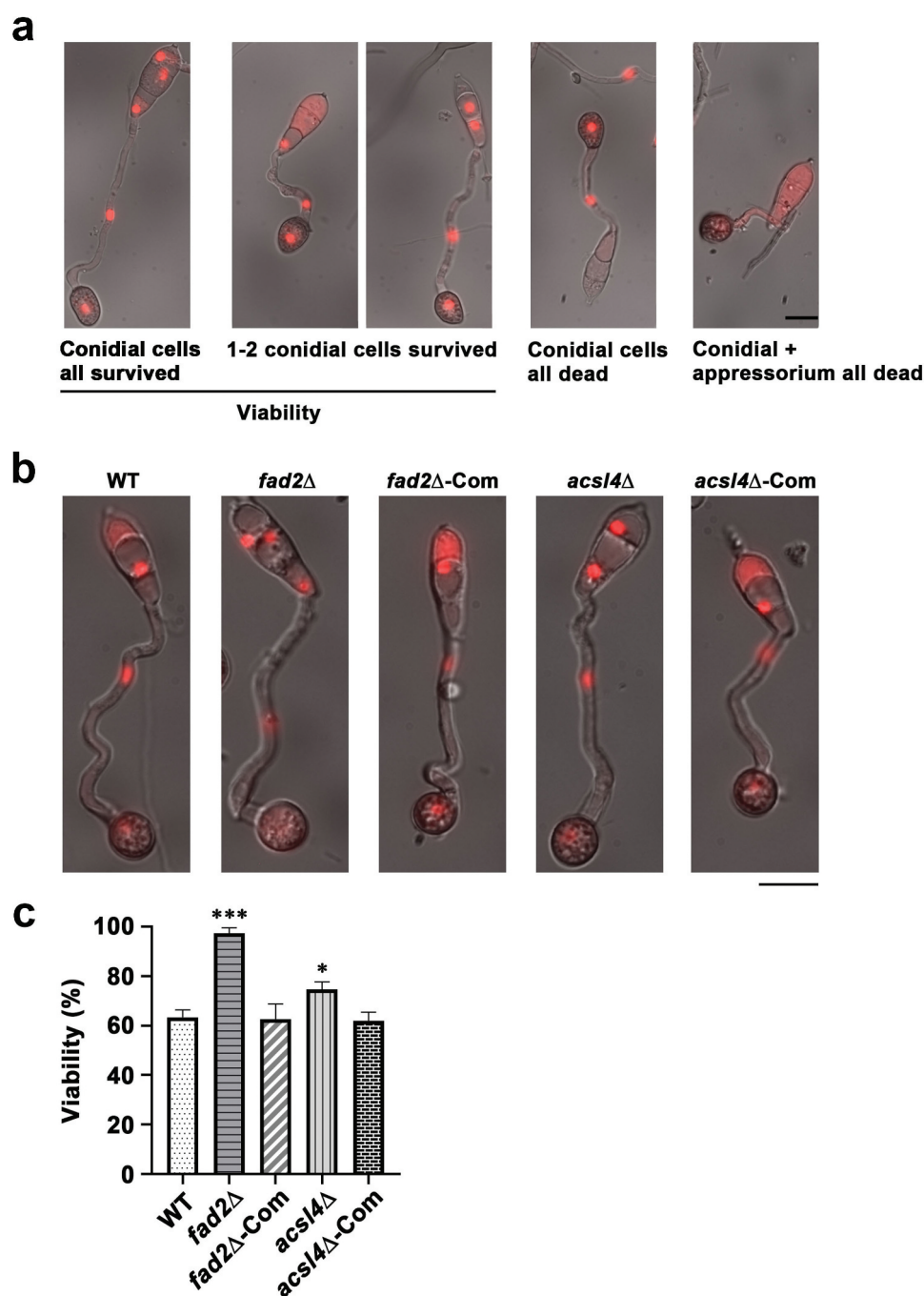


**Figure 3.** Fad2 and Acsl4 regulate cell death in *Magnaporthe oryzae*. (a) Microscopic images of H1-RFP expressing strain, demonstrating sequential death of conidial cells during appressorium formation. Scale bar = 10  $\mu$ m. (b) Conidia of WT, *fad2Δ*, *fad2Δ*-Com, *acs14Δ*, or *acs14Δ*-Com strains expressing the nucleus marker H1-RFP were allowed to germinate on the inductive surface for 14.5 h, and fluorescent microscopy was performed to visualize nuclei. Scale bar = 10  $\mu$ m. (c) Conidia viability was quantified based on H1-RFP marked nuclei, at 14.5 hpi. “Conidial cells all survived” and “1–2 conidial cells survived” demonstrated in (a) were considered as viability. Mean  $\pm$  S.D. was derived from three independent repeats ( $n \geq 50$  conidia each) for each treatment. \* or \*\*\*:  $p < 0.05$  or  $p < 0.001$  vs WT (Student’s *t*-test).

Stockwell 2017). Consistently, we found that MDA contents were significantly lower in *fad2Δ* or *acs14Δ* conidia compared to WT (Figure 4c). Levels of MDA contents

were fully restored in the *fad2Δ*-Com or *acs14Δ*-Com strain, confirming that Fad2 and Acsl4 are required for proper lipid peroxidation.

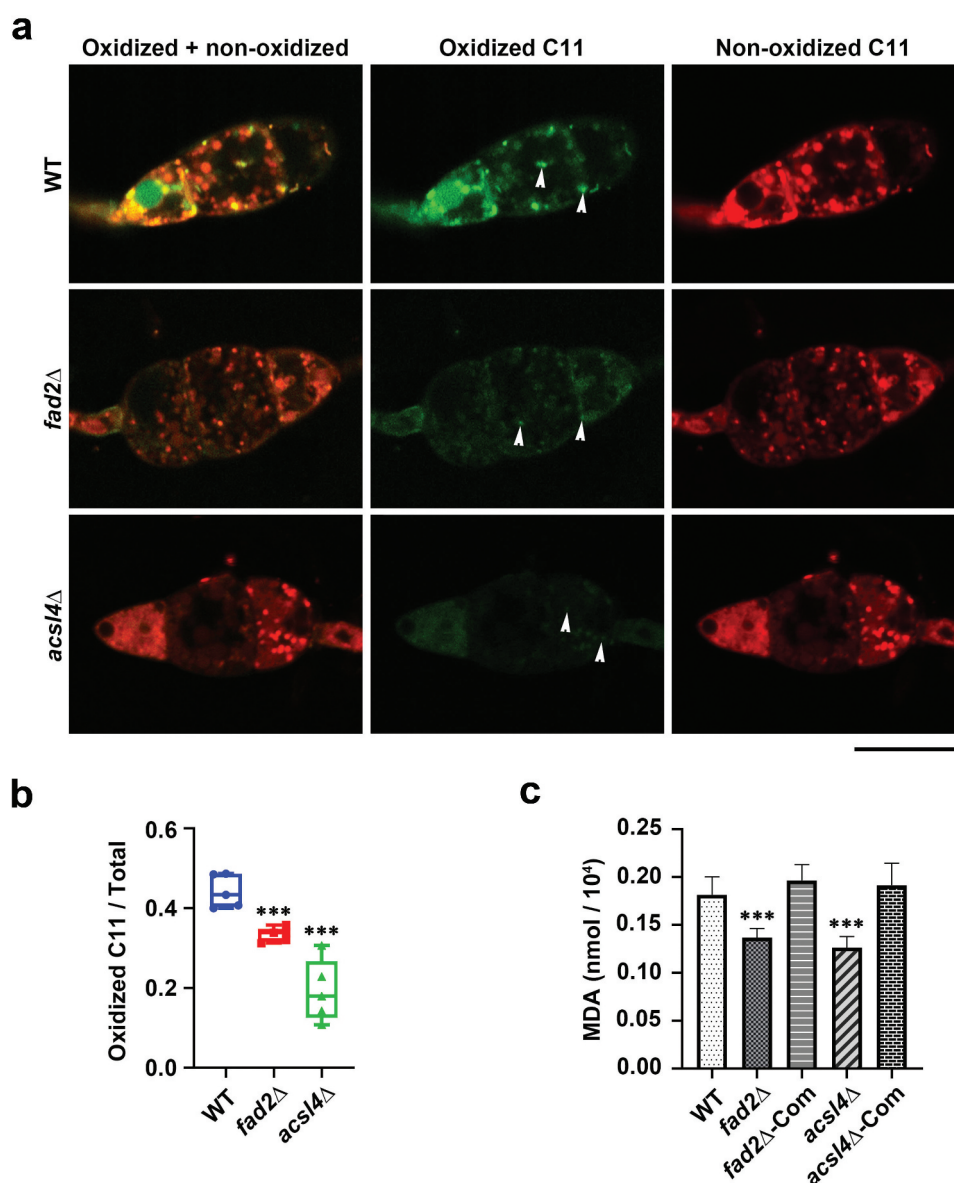


**Figure 4.** Fad2 and Acsl4 contribute to PUFA-PLs biosynthesis and lipid peroxidation in *Magnaporthe oryzae*. (a) Conidia (2,000 per droplet) were inoculated on hydrophobic coverslips for 7 h and then stained with 10  $\mu\text{mol/L}$  C11-BODIPY<sup>581/591</sup> for 30 min to monitor the oxidized and nonoxidized variants of lipid peroxides. Arrows denote examples of oxidized C11 signals accumulated on cellular membranes. Scale bar = 10  $\mu\text{m}$ . (b) Quantitative analysis of lipid peroxidation extent indicated by mean fluorescence intensity (MFI) ratio of oxidised (green fluorescence) to total fluorescence (green plus red). The MFI of either green or red fluorescence in single conidia was assessed using the “measurement” function of ImageJ software. For each instance,  $n \geq 5$  conidia were included for quantitative analysis. \*\*\*:  $p < 0.001$  vs WT (Student’s  $t$ -test). (c) MDA concentrations of WT, *fad2*Δ, *fad2*Δ-Com, *acsl4*Δ, or *acsl4*Δ-Com conidia were measured at 6 hpi. Mean  $\pm$  S.D. was derived from three independent biological repeats, each containing  $9 \times 10^6$  conidia. \*\*\*:  $p < 0.001$  vs WT (Student’s  $t$ -test).

### 3.4. Fad2 and Acsl4 mediated lipid metabolism contributes to *M. oryzae* pathogenicity

Given that Fad2 and Acsl4 are involved in lipid peroxidation required for induction of ferroptosis, we next performed a lipidomic analysis based on UHPLC-HRMS/MS analysis with developing conidia (6 hpi on the inductive surface) of WT, *fad2*Δ, and *acsl4*Δ mutant. The result

(Suppl Dataset S1) showed that multiple species of PUFA-PLs, including phosphatidylinositol (PI), phosphatidylserine (PS), phosphatidylethanolamine (PE), and phosphatidylcholine (PC), etc., were all significantly decreased ( $|\text{Log2FC}| \geq 0.26$ ,  $p < 0.05$ ) in the developing conidia of *fad2*Δ or *acsl4*Δ mutant, compared to WT conidia (6 h, Figure 5a–b). A total of 14 types of PE

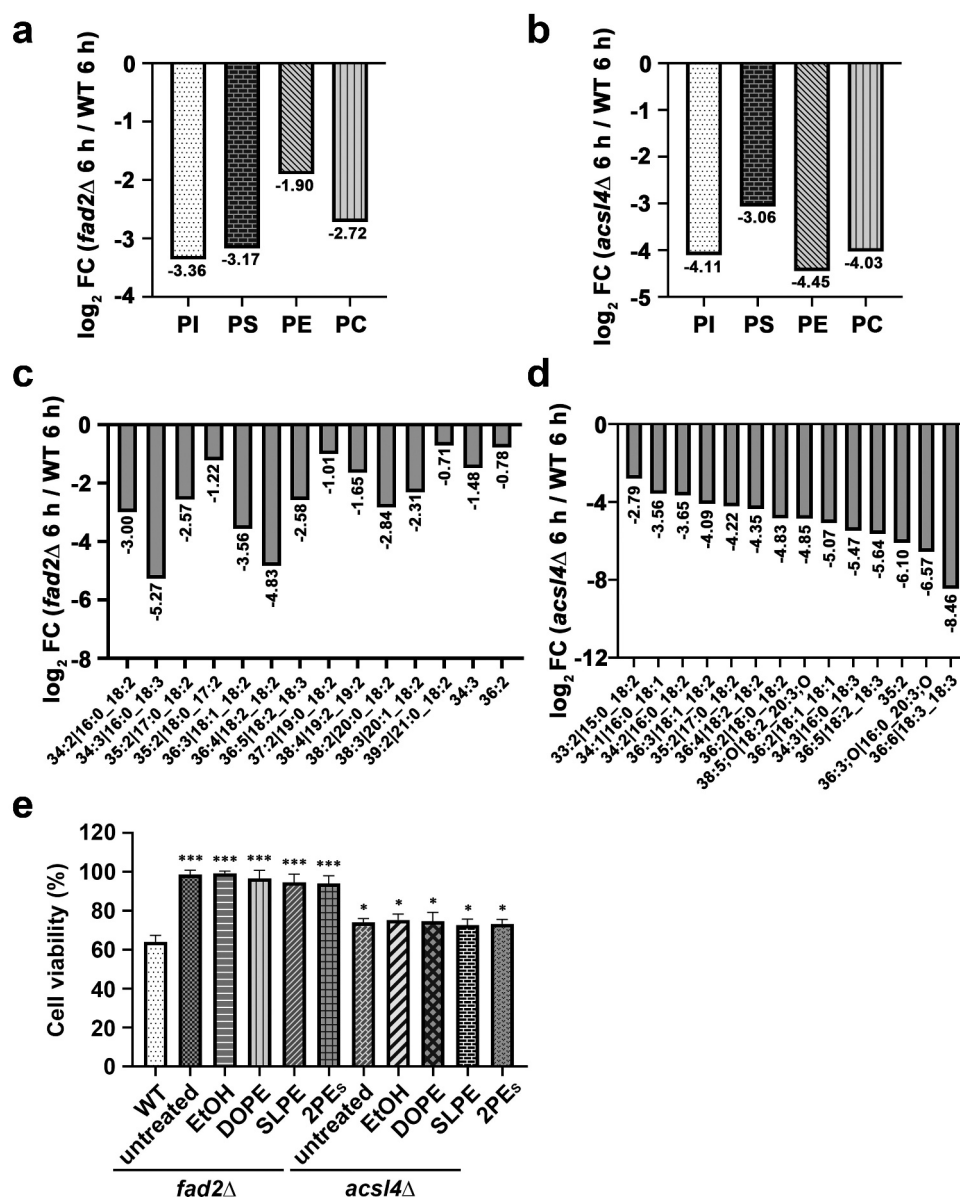


**Figure 5.** Fad2 and Acsl4 are involved in PUFA biosynthesis. PI, PS, PE, and PC species were significantly decreased in *fad2* $\Delta$  (a) or *acs4* $\Delta$  (b) conidia at 6 h, as compared to WT. 14 types of PE were significantly decreased in *fad2* $\Delta$  (c) or *acs4* $\Delta$  (d) conidia at 6 h, as compared to WT. (e) Conidial viability of WT, *fad2* $\Delta$ , or *acs4* $\Delta$  was quantified based on H1-RFP marked nuclei, at 14.5 hpi. DOPE (20  $\mu$ mol/L), SLPE (20  $\mu$ mol/L), or in combination (v:v = 1:1) were added at 0 h. EtOH (0.2%) served as a solvent control. Mean  $\pm$  S.D. was derived from three independent repeats ( $n \geq 50$  conidia each) for each treatment. \* or \*\*\*:  $p < 0.05$  or  $p < 0.001$  vs WT (viability) (Student's  $t$ -test).

were significantly decreased in *fad2* $\Delta$  or *acs4* $\Delta$  respectively, compared to the WT conidia (Figure 5c–d). This result confirms that Fad2 and Acsl4 are involved in the production of PUFA-PLs, which may serve as substrates for oxidation reactions (lipid peroxidation) and thus trigger ferroptosis.

We further tested the effect of PEs on cell death induction in the *fad2* $\Delta$  or *acs4* $\Delta$  conidia by feeding the available PUFA-PLs, DOPE (1,2-Dioleoyl-sn-glycero-3-phosphoethanolamine), or SLPE to the *fad2* $\Delta$  or *acs4* $\Delta$  conidia inoculated on inductive surface. At 14.5 h, DOPE or SLPE could not promote conidial cell death that was defective in *fad2* $\Delta$  or *acs4* $\Delta$  mutants, either supplied individually or

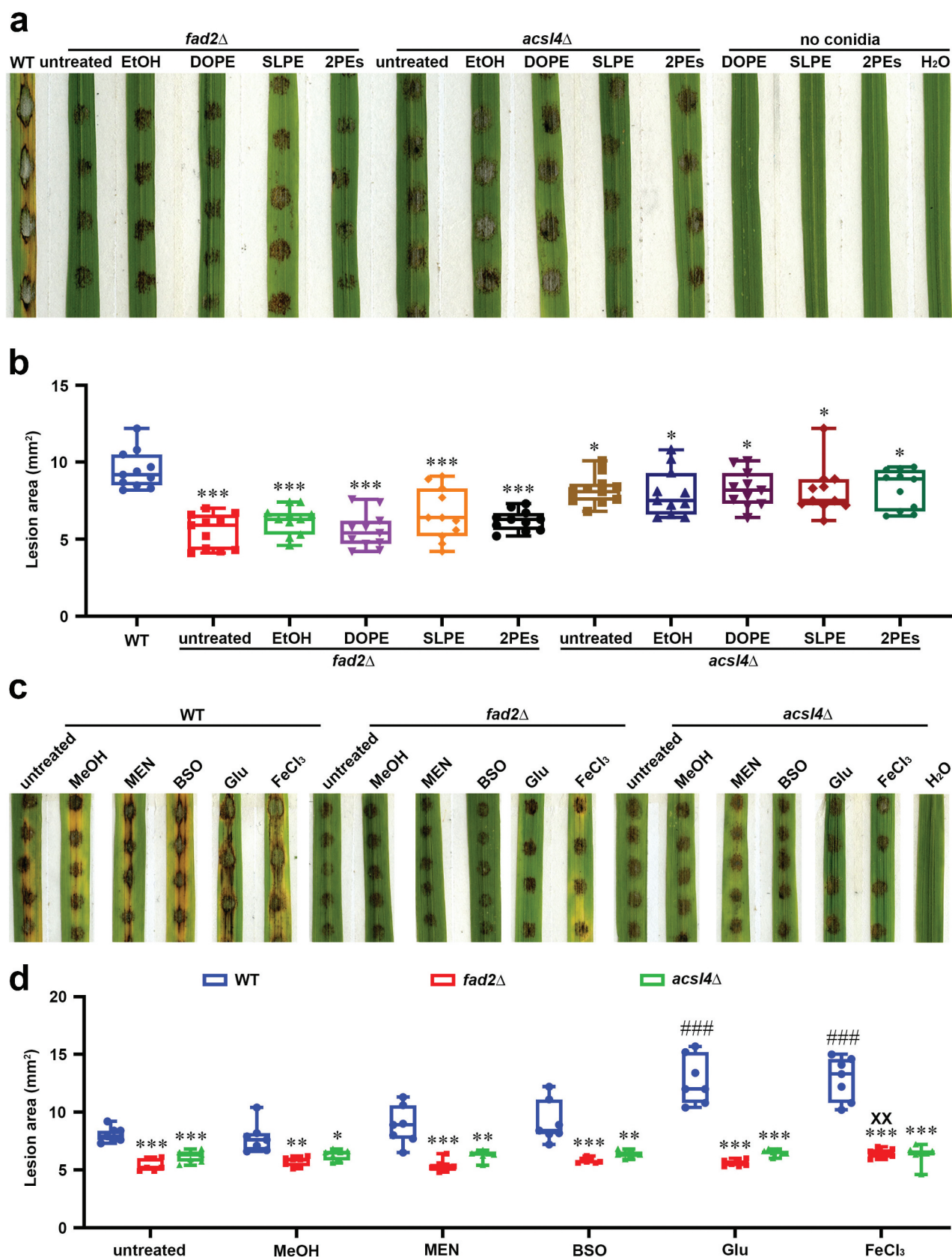


**Figure 6.** Effect of PEs and ferroptosis inducers on *Magnaporthe oryzae* pathogenicity. (a) WT, *fad2Δ*, or *acs14Δ* conidia (2,000 per droplet) were inoculated on the detached rice leaves for pathogenicity assay. Treatment with DOPE (20 μmol/L) or SLPE (20 μmol/L) individually, or in combination (v:v = 1:1). Inoculation of the different PEs or H<sub>2</sub>O on the rice leaves without conidia served as blank controls. EtOH (0.2%) served as a solvent control. (b) Box plots depict lesion area caused by



in combination (v:v = 1:1; Figure 5e). Correspondingly, DOPE or SLPE could not restore the pathogenicity defect of *fad2Δ* or *acsl4Δ*, either supplied individually or in combination (Figure 6a–b). This implies that the defective conidial death and pathogenicity of these 2 mutants are caused by deficiency of other species of PUFAs than DOPE or SLPE that depends on Fad2 or Acsl4 for biosynthesis.

We further tested the effect of ferroptosis inducers, including the oxidative agents buthionine sulfoximine (BSO) and menadione (MEN), as well as glutamate (Glu) and FeCl<sub>3</sub>, on the pathogenicity of WT or mutant conidia. All four tested ferroptosis inducers failed to restore the pathogenicity of *acsl4Δ* (Figure 6c–d). FeCl<sub>3</sub> could slightly promote lesion formation by *fad2Δ* conidia on the infected leaves, but other chemicals seemed to have no such effect (Figure 6c).

Overall, our results show that Fad2 and Acsl4 are involved in lipid peroxidation and the consequent ferroptotic death of the developing conidia, likely by providing PUFA-PLs as substrates for oxidation.

### 3.5. Screening for potential interacting proteins of Fad2

By yeast-two-hybrid screen using a cDNA library of *M. oryzae*, we identified 54 proteins potentially interacting with Fad2 (Table 1). The potential Fad2-interacting proteins were enriched in metabolism, genetic information processing, and cellular processes (Figure S3A). The top 25 enriched KEGG pathways include the C5-branched dibasic acid metabolism pathway and glutathione metabolism pathway (Figure S3B; Suppl Dataset S2), which contain the genes with reported function involved in appressorium formation and pathogenicity in *M. oryzae* (Jeon et al. 2007; Du et al. 2013).

Among the potential Fad2-interacting proteins, we noticed several membrane-localised proteins including calcium-binding protein (MGG\_01607) located on endoplasmic reticulum (ER), transport channel (MGG\_00406) in mitochondrial membranes, MFS phospholipid transporter Git1 (MGG\_00464), ammonium transporter MEP1 (MGG\_00537); high-affinity glucose transporter RGT2 (MGG\_06203); and multidrug resistance-associated protein 2 (MGG\_08309). Proteins involved in redox homeostasis were among Fad2-interacting proteins, including NADPH dehydrogenase (MGG\_04569), flavohemoglobin (MGG\_00198), glucose-6-phosphate 1-dehydrogenase (MGG\_09926), glutathione S-transferase Gst3 (MGG\_01410), and cytochrome c oxidase subunit 6B (MGG\_01111). Analyses of Fad2-interacting proteins suggest that Fad2 may localise on the cellular membrane and contribute to cellular redox homeostasis. Overall, these candidate interacting proteins provide a clue to the mechanism of Fad2 regulating fungal cell growth, differentiation, death, and pathogenicity.

### 3.6. Sub-cellular localization of Fad2-GFP and Acsl4-GFP

By using the genetic complementation expressing Fad2-GFP or Acsl4-GFP, we investigated the sub-cellular localisation of these two proteins. Under confocal microscopy, Fad2-GFP appeared localised on punctate or filamentous structures (Figure 7a), likely corresponding to the intracellular compartments in which PUFAs are produced by forming the unsaturated bonds catalysed by the Fad2 enzyme. Acsl4-GFP seemed distributed in cytosol, but also accumulated on some punctate compartments (Figure 7b), likely representing the sites

---

WT or mutant conidia under different treatments, at 5 dpi ( $n = 11$ ). At least two independent biological repeats were performed for each instance, \* or \*\*\*:  $p < 0.05$  or  $p < 0.001$  vs WT (Student's *t*-test). (c) Infection of rice leaves by WT, *fad2Δ*, or *acsl4Δ* conidia (2,000 per inoculum) in the presence of MEN (10 μmol/L), BSO (100 μmol/L), glu (100 μmol/L), or FeCl<sub>3</sub> (5 μmol/L). Inoculation of the H<sub>2</sub>O on the rice leaves without conidia served as blank controls. MeOH (0.1%) serves as solvent control. (d) Box plots depict lesion area caused by WT or mutant conidia under different treatments, at 5 dpi ( $n = 7$ ). At least two independent biological repeats were performed for each instance, \*, \*\* or \*\*\*:  $p < 0.05$ ,  $p < 0.01$  or  $p < 0.001$ , mutant vs WT under different treatments. \*\*\*:  $p < 0.001$ , WT under different treatments respectively vs untreated WT. \*\*:  $p < 0.01$ , mutant under different treatment respectively vs untreated condition (Student's *t*-test). For (a) and (c), infected leaves were kept in the constant dark for 24 h, and then in the incubator with cyclic dark:light (12 h:12 h) settings for 5 d before examination and photographing of disease lesions.

**Table 1.** Potential Fad2-associating proteins.

Gene ID	Annotation (reference)
MGG_03671	Uncharacterized protein
MGG_03577	Histone H2A
MGG_00505	Septation protein SUN4 Saitoh et al. (2012)
MGG_00464	MFS phospholipid transporter Git1
MGG_17792	Uncharacterized protein
MGG_01159	Histone H3
MGG_05638	Uncharacterized protein
MGG_00537	Ammonium transporter MEP1 Jeon et al. (2007)
MGG_09926	Glucose-6-phosphate 1-dehydrogenase Jeon et al. (2007)
MGG_04569	NADPH dehydrogenase
MGG_01609	Uncharacterized protein Saitoh et al. (2012)
MGG_01608	Methylthioribulose-1-phosphate dehydratase
MGG_06958	Hsp70-like protein
MGG_06204	Uncharacterized protein Jeon et al. (2007)
MGG_01256	Phosphoribosylaminoimidazole carboxylase
MGG_03945	Acetolactate synthase
MGG_12316	Uncharacterized protein
MGG_04156	Aspartate aminotransferase
MGG_16298	Uncharacterized protein
MGG_01607	Calnexin
MGG_05155	Adenosylhomocysteinase
MGG_16375	Aldehyde reductase
MGG_17655	Uncharacterized protein
MGG_15916	Uncharacterized protein
MGG_17308	Uncharacterized protein
MGG_17554	Uncharacterized protein
MGG_17619	Uncharacterized protein
MGG_17538	Uncharacterized protein
MGG_15154	Uncharacterized protein
MGG_00406	Mitochondrial import inner membrane translocase subunit tim-16
MGG_16862	Uncharacterized protein
MGG_00198	Flavohemoglobin
MGG_15479	Uncharacterized protein
MGG_11701	Uncharacterized protein
MGG_11336	Uncharacterized protein
MGG_05233	Uncharacterized protein
MGG_03696	CMGC/CK2 protein kinase Zhang et al. (2019)
MGG_01045	Arrestin domain-containing protein
MGG_02854	Pirin domain-containing protein
MGG_08309	Multidrug resistance-associated protein 2
MGG_05673	40S ribosomal protein S3
MGG_06907	Uncharacterized protein
MGG_06908	DNA polymerase beta
MGG_01410	Glutathione S-transferase Gst3 Jeon et al. (2007)
MGG_04736	Uncharacterized protein
MGG_01104	Acetolactate synthase small subunit Du et al. (2013)
MGG_00546	60S ribosomal protein L44
MGG_07877	Dipeptidyl-peptidase V
MGG_06203	High-affinity glucose transporter RGT2 Jeon et al. (2007)
MGG_01111	Cytochrome c oxidase subunit 6B
MGG_01632	Uncharacterized protein
MGG_01631	UTP-glucose-1-phosphate uridylyltransferase
MGG_13474	Eukaryotic translation initiation factor eif-1
MGG_00223	Fructose-bisphosphate aldolase 1

where the Acsl4 enzyme catalyses the incorporation of PUFAs into the phospholipid bilayer of cell membranes.

### 3.7. *Fad2* and *Acsl4* are involved in stress tolerance

We further evaluated the stress tolerance of WT or mutants, by assessing their mycelial growth under salt stress (CM containing 0.7 mol/L NaCl or 1 mol/L

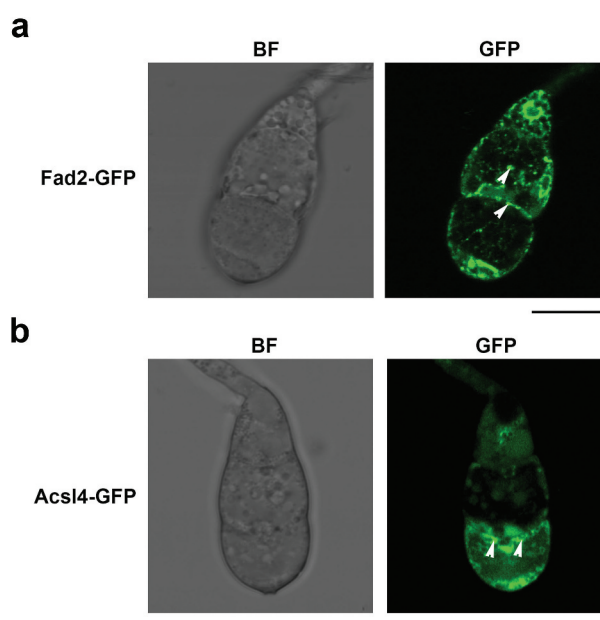


**Figure 7.** Subcellular localisation of Fad2-GFP and Acsl4-GFP. Confocal microscopy was performed using conidia of the complementation strains expressing Fad2-GFP (a) or Acsl4-GFP (b) fusion proteins. Scale bar = 10 µm.

KCl), osmotic stress (1 mol/L sorbitol), oxidative stress (5 mmol/L H<sub>2</sub>O<sub>2</sub>), or cell-wall-perturbing reagents [0.01% sodium dodecyl sulphate (SDS) or 0.2 mg/mL Congo red (CR)]. The results showed that *fad2Δ* was hypersensitive to cell-wall stress caused by CR treatment, and *acsl4Δ* was less sensitive to oxidative stress, compared to the WT mycelia (Figure S4A–B). These results display that *M. oryzae* *FAD2* and *ACSL4* play important, yet differential roles, in response to different environmental stresses.

## 4. Discussion

PUFA-PLs are highly susceptible to lipid peroxidation under oxidative stress, leading to ferroptotic cell death (Yang et al. 2022). Biosynthesis of PUFA-PLs involves fatty acid desaturases (FADs), a class of oxygen-dependent enzymes that dehydrogenate C–C bonds in the fatty acids, thus producing PUFAs (Pereira et al. 2003; Santomartino et al. 2017; Starikov et al. 2020; Xiao et al. 2022), and acyl-coenzyme A synthetases long-chain isoform (ACSL) enzymes, that ligate PUFAs to phospholipids (Tomitsuka et al. 2023). In *M. oryzae*, we identified orthologous Fad2 and Acsl4 enzymes and confirmed that they were involved in the

biosynthesis of PUFA-PLs including PI, PC, PS, and PE, based on lipidomics analysis (Figure 5a–b).

*FADS2* gene (animal ortholog of *FAD2*) was shown to be up-regulated in breast cancer, lung cancer, brain cancer, etc., and able to promote tumour aggressiveness while negatively regulating ferroptosis (He et al. 2012; Jiang et al. 2017; Li et al. 2020; Xuan et al. 2022). In contrast, *FADS2*-dependent biosynthesis of PUFA was shown to be required for the induction of lipid peroxidation and ferroptosis, playing a role in defending against hepatitis C virus (HCV) (Yamane et al. 2022). On the other hand, *ACSL4* facilitates the incorporation of PUFAs in the phospholipid bilayer of cell membranes, thus increasing the sensitivity of multiple cancer cells to ferroptosis (Doll et al. 2017; Wu et al. 2019; Cheng et al. 2020). Our previous study has proved that ferroptotic death of the developing conidia is critical for appressorium formation and function in *M. oryzae*, thus contributing to fungal pathogenicity (Shen et al. 2020). This study shows that *M. oryzae* *Fad2* and *Acsl4* orthologs contribute to PUFA-PLs biosynthesis, leading to ferroptotic cell death of the developing conidia. This represents the first report on the role of PUFA-PLs in fungal ferroptosis. In addition, we found that invasive growth was delayed or blocked in the *fad2Δ* and *acsl4Δ* mutants (Figure 2d), while the generation of pressure turgor in the appressorium seemed not affected (Figure 2c). We infer that the defected appressorium-mediated host infection may be due to the delayed/compromised cell death (ferroptosis) of the developing conidia.

However, when supplied with DOPE, SLPE, or both, to the *fad2Δ* or *acsl4Δ* conidia, the defects in conidial death or pathogenicity were not restored (Figures 5e and 6a–b). We infer that loss of either one of these two genes caused a reduction in PUFA-PLs levels, including but not limited to DOPE and SLPE. A total of 14 PE species were decreased in these two mutants (Figure 5c–d). Other PUFA-PL species that depend on *Fad2*/*Acsl4* for biosynthesis may be also necessary for ferroptosis induction and pathogenicity. Alternatively, *Fad2*/*Acsl4* may contribute to *M. oryzae* pathogenicity via other pathways besides PUFA-PLs production. Particularly, we notice that *Fad2* may potentially interact with proteins involved in cellular redox homeostasis (Table 1), suggesting that *Fad2* may not only provide lipid substrates but also be involved in generating an elevated oxidative status to cause lipid peroxidation. Supporting this hypothesis, our result showed

that treatment with  $\text{FeCl}_3$ , an oxidative agent to causes lipid peroxidation, could partially restore *fad2Δ* pathogenicity (Figure 6c–d).

We further identified potential *Fad2*-interacting proteins by yeast-two-hybrid screening with *M. oryzae* cDNA library. The identified proteins include ammonium transporter MEP1, glucose-6-phosphate 1-dehydrogenase, high-affinity glucose transporter RGT2, and glutathione S-transferase Gst3, which were reported to be important for appressorium formation and host infection (Jeon et al. 2007). It is worth further investigating on interaction and functional relevance between *Fad2* and these regulators of *M. oryzae* pathogenicity.

It has been reported that plant *Fad2* localises to the endoplasmic reticulum (ER) membrane (McCartney et al. 2004). On the other hand, *Acsl4* was found localising on the plasma membrane, or in the cytosol, ER, and lipid droplets, of animal cells or tumour cells (Küch et al. 2014; Ndiaye et al. 2020). In this study, we found that *Fad2*-GFP appeared localised on punctate or filamentous structures, and *Acsl4*-GFP seemed distributed in cytosol and occasionally accumulated on punctate compartments (Figure 7a–b). We speculate that these *Fad2*- or *Acsl4*- associated intracellular compartments, whose identity awaits elucidation, may be related to lipid metabolism.

## 5. Conclusions

Overall, our study revealed the biological function of PUFA biosynthesis enzyme *Fad2* and PUFA-CoA ligase *Acsl4*, in *M. oryzae* growth, asexual development, and pathogenesis. Particularly, *Fad2* and *Acsl4* contribute to the induction of ferroptotic death of the developing conidia, likely by providing PUFA-PLs as substrates for lipid peroxidation, and thus play a crucial role in fungal pathogenicity. These findings will certainly broaden our understanding of the metabolic adaptation of fungal cells during pathogenic development and provide a theoretical basis for designing an efficient disease management strategy.

## Acknowledgments

We would like to thank Dr Shi Bihai from the Confocal Microscopy Facility for helping us with confocal microscopy observation and imaging.

## Disclosure statement

No potential conflict of interest was reported by the author(s).

## Funding

This work is supported by the National Key Research and Development Program of China [2022YFA1304402], and the National Natural Science Foundation of China [32022070, 31970139] to YZ. Deng. The funders had no role in study design, data collection, and interpretation, or the decision to submit the work for publication.

## ORCID

Zhibin Liang  <http://orcid.org/0000-0003-3433-0975>

Yi Zhen Deng  <http://orcid.org/0000-0002-3572-1559>

## References

- Callaway E. 2016. Devastating wheat fungus appears in Asia for first time. *Nature*. 532(7600):421–2. doi: [10.1038/532421a](https://doi.org/10.1038/532421a).
- Carlsen CU, Kurtmann L, Brüggemann DA, Hoff S, Risbo J, Skibsted LH. 2009. Investigation of oxidation in freeze-dried membranes using the fluorescent probe C11-BODIPY(581/591). *Cryobiology*. 58(3):262–267. doi: [10.1016/j.cryobiol.2009.01.005](https://doi.org/10.1016/j.cryobiol.2009.01.005).
- Cheng J, Fan YQ, Liu BH, Zhou H, Wang JM, Chen QX. 2020. ACSL4 suppresses glioma cells proliferation via activating ferroptosis. *Oncol Rep*. 43(1):147–158. doi: [10.3892/or.2019.7419](https://doi.org/10.3892/or.2019.7419).
- Dai Y, Chen Y, Mo D, Jin R, Huang Y, Zhang L, Zhang C, Gao H, Yan Q. 2023a. Inhibition of ACSL4 ameliorates tubular ferroptotic cell death and protects against fibrotic kidney disease. *Commun Biol*. 6(1):907. doi: [10.1038/s42003-023-05272-5](https://doi.org/10.1038/s42003-023-05272-5).
- Dai Z, Zhang W, Zhou L, Huang J. 2023b. Probing lipid peroxidation in ferroptosis: emphasizing the utilization of C11-BODIPY-based protocols. *Methods Mol Biol*. 2712:61–72. doi: [10.1007/978-1-0716-3433-2\\_6](https://doi.org/10.1007/978-1-0716-3433-2_6).
- Dangol S, Chen Y, Hwang BK, Jwa NS. 2019. Iron- and reactive oxygen species-dependent ferroptotic cell death in rice-*Magnaporthe oryzae* interactions. *Plant Cell*. 31(1):189–209. doi: [10.1105/tpc.18.00535](https://doi.org/10.1105/tpc.18.00535).
- Dar AA, Choudhury AR, Kancharla PK, Arumugam N. 2017. The FAD2 gene in plants: occurrence, regulation, and role. *Front Plant Sci*. 8:1789. doi: [10.3389/fpls.2017.01789](https://doi.org/10.3389/fpls.2017.01789).
- Dean R, Van Kan JA, Pretorius ZA, Hammond-Kosack KE, Di Pietro A, Spanu PD, Rudd JJ, Dickman M, Kahmann R, Ellis J, et al. 2012. The top 10 fungal pathogens in molecular plant pathology. *Mol Plant Pathol*. 13(4):414–430. doi: [10.1111/j.1364-3703.2011.00783.x](https://doi.org/10.1111/j.1364-3703.2011.00783.x).
- Dean RA. 1997. Signal pathways and appressorium morphogenesis. *Annu Rev Phytopathol*. 35(1):211–234. doi: [10.1146/annurev.phyto.35.1.211](https://doi.org/10.1146/annurev.phyto.35.1.211).
- Ding K, Liu C, Li L, Yang M, Jiang N, Luo S, Sun L. 2023. Acyl-CoA synthase ACSL4: an essential target in ferroptosis and fatty acid metabolism. *Chin Med J (Engl)*. 136(21):2521–2537. doi: [10.1097/cm9.0000000000002533](https://doi.org/10.1097/cm9.0000000000002533).
- Distéfano AM, Martin MV, Córdoba JP, Bellido AM, D'Ippólito S, Colman SL, Soto D, Roldán JA, Bartoli CG, Zabaleta EJ, et al. 2017. Heat stress induces ferroptosis-like cell death in plants. *J Cell Biol*. 216(2):463–476. doi: [10.1083/jcb.201605110](https://doi.org/10.1083/jcb.201605110).
- Dixon SJ, Lemberg KM, Lamprecht MR, Skouta R, Zaitsev EM, Gleason CE, Patel DN, Bauer AJ, Cantley AM, Yang WS, et al. 2012. Ferroptosis: an iron-dependent form of non-apoptotic cell death. *Cell*. 149(5):1060–1072. doi: [10.1016/j.cell.2012.03.042](https://doi.org/10.1016/j.cell.2012.03.042).
- Doll S, Proneth B, Tyurina YY, Panzilius E, Kobayashi S, Ingold I, Irmeler M, Beckers J, Aichler M, Walch A, et al. 2017. ACSL4 dictates ferroptosis sensitivity by shaping cellular lipid composition. *Nat Chem Biol*. 13(1):91–98. doi: [10.1038/nchembio.2239](https://doi.org/10.1038/nchembio.2239).
- Drummen GP, van Liebergen LC, Op den Kamp JAF, Post JA. 2002. C11-BODIPY(581/591), an oxidation-sensitive fluorescent lipid peroxidation probe: (micro)spectroscopic characterization and validation of methodology. *Free Radic Biol Med*. 33(4):473–490. doi: [10.1016/s0891-5849\(02\)00848-1](https://doi.org/10.1016/s0891-5849(02)00848-1).
- Du Y, Zhang H, Hong L, Wang J, Zheng X, Zhang Z. 2013. Acetolactate synthases Mollv2 and Mollv6 are required for infection-related morphogenesis in *Magnaporthe oryzae*. *Mol Plant Pathol*. 14(9):870–884. doi: [10.1111/mpp.12053](https://doi.org/10.1111/mpp.12053).
- Dufresne M, Osbourn AE. 2001. Definition of tissue-specific and general requirements for plant infection in a phytopathogenic fungus. *Mol Plant Microbe Interact*. 14(3):300–307. doi: [10.1094/mpmi.2001.14.3.300](https://doi.org/10.1094/mpmi.2001.14.3.300).
- Egan MJ, Wang ZY, Jones MA, Smirnoff N, Talbot NJ. 2007. Generation of reactive oxygen species by fungal NADPH oxidases is required for rice blast disease. *Proc Natl Acad Sci USA*. 104(28):11772–11777. doi: [10.1073/pnas.0700574104](https://doi.org/10.1073/pnas.0700574104).
- Fernandez J, Orth K. 2018. Rise of a cereal killer: the biology of *Magnaporthe oryzae* biotrophic growth. *Trends Microbiol*. 26(7):582–597. doi: [10.1016/j.tim.2017.12.007](https://doi.org/10.1016/j.tim.2017.12.007).
- Foster AJ, Ryder LS, Kershaw MJ, Talbot NJ. 2017. The role of glycerol in the pathogenic lifestyle of the rice blast fungus *Magnaporthe oryzae*. *Environ Microbiol*. 19(3):1008–1016. doi: [10.1111/1462-2920.13688](https://doi.org/10.1111/1462-2920.13688).
- Gaschler MM, Stockwell BR. 2017. Lipid peroxidation in cell death. *Biochem Biophys Res Commun*. 482(3):419–425. doi: [10.1016/j.bbrc.2016.10.086](https://doi.org/10.1016/j.bbrc.2016.10.086).
- Hamer JE, Howard RJ, Chumley FG, Valent B. 1988. A mechanism for surface attachment in spores of a plant pathogenic fungus. *Science*. 239(4837):288–290. doi: [10.1126/science.239.4837.288](https://doi.org/10.1126/science.239.4837.288).
- He C, Qu X, Wan J, Rong R, Huang L, Cai C, Zhou K, Gu Y, Qian SY, Kang JX, et al. 2012. Inhibiting delta-6 desaturase activity suppresses tumor growth in mice. *PLoS One*. 7(10):e47567. doi: [10.1371/journal.pone.0047567](https://doi.org/10.1371/journal.pone.0047567).
- Howard RJ, Ferrari MA, Roach DH, Money NP. 1991. Penetration of hard substrates by a fungus employing enormous turgor



- pressures. *Proc Natl Acad Sci USA*. 88(24):11281–11284. doi: [10.1073/pnas.88.24.11281](https://doi.org/10.1073/pnas.88.24.11281).
- Howard RJ, Valent B. 1996. Breaking and entering: host penetration by the fungal rice blast pathogen *Magnaporthe grisea*. *Annu Rev Microbiol*. 50(1):491–512. doi: [10.1146/annurev.micro.50.1.491](https://doi.org/10.1146/annurev.micro.50.1.491).
- Jeon J, Park SY, Chi MH, Choi J, Park J, Rho HS, Kim S, Goh J, Yoo S, Choi J, et al. 2007. Genome-wide functional analysis of pathogenicity genes in the rice blast fungus. *Nat Genet*. 39(4):561–565. doi: [10.1038/ng2002](https://doi.org/10.1038/ng2002).
- Jiang Y, Mao C, Yang R, Yan B, Shi Y, Liu X, Lai W, Liu Y, Wang X, Xiao D, et al. 2017. EGLN1/c-myc induced lymphoid-specific helicase inhibits ferroptosis through lipid metabolic gene expression changes. *Theranostics*. 7(13):3293–3305. doi: [10.7150/thno.19988](https://doi.org/10.7150/thno.19988).
- Jofre-Monseny L, de Pascual-Teresa S, Plonka E, Huebbe P, Boesch-Saadatmandi C, Miniñane AM, Rimbach G. 2007. Differential effects of apolipoprotein E3 and E4 on markers of oxidative status in macrophages. *Br J Nutr*. 97(5):864–871. doi: [10.1017/s0007114507669219](https://doi.org/10.1017/s0007114507669219).
- Kagan VE, Mao G, Qu F, Angeli JP, Doll S, Croix CS, Dar HH, Liu B, Tyurin VA, Ritov VB, et al. 2017. Oxidized arachidonic and adrenic PEs navigate cells to ferroptosis. *Nat Chem Biol*. 13(1):81–90. doi: [10.1038/nchembio.2238](https://doi.org/10.1038/nchembio.2238).
- Kankanala P, Czymmek K, Valent B. 2007. Roles for rice membrane dynamics and plasmodesmata during biotrophic invasion by the blast fungus. *Plant Cell*. 19(2):706–724. doi: [10.1105/tpc.106.046300](https://doi.org/10.1105/tpc.106.046300).
- Koelmel JP, Kroeger NM, Ulmer CZ, Bowden JA, Patterson RE, Cochran JA, Beecher CWW, Garrett TJ, Yost RA. 2017. LipidMatch: an automated workflow for rule-based lipid identification using untargeted high-resolution tandem mass spectrometry data. *BMC Bioinf*. 18(1):331. doi: [10.1186/s12859-017-1744-3](https://doi.org/10.1186/s12859-017-1744-3).
- Küch EM, Vellaramkalayil R, Zhang I, Lehnen D, Brügger B, Sreemmel W, Eehalt R, Poppelreuther M, Füllekrug J. 2014. Differentially localized acyl-CoA synthetase 4 isoenzymes mediate the metabolic channeling of fatty acids towards phosphatidylinositol. *Biochim Biophys Acta*. 1841(2):227–239. doi: [10.1016/j.bbalip.2013.10.018](https://doi.org/10.1016/j.bbalip.2013.10.018).
- Lee JY, Nam M, Son HY, Hyun K, Jang SY, Kim JW, Kim MW, Jung Y, Jang E, Yoon SJ, et al. 2020. Polyunsaturated fatty acid biosynthesis pathway determines ferroptosis sensitivity in gastric cancer. *Proc Natl Acad Sci USA*. 117(51):32433–32442. doi: [10.1073/pnas.2006828117](https://doi.org/10.1073/pnas.2006828117).
- Li Y, Feng D, Wang Z, Zhao Y, Sun R, Tian D, Liu D, Zhang F, Ning S, Yao J, et al. 2019. Ischemia-induced ACSL4 activation contributes to ferroptosis-mediated tissue injury in intestinal ischemia/reperfusion. *Cell Death Differ*. 26(11):2284–2299. doi: [10.1038/s41418-019-0299-4](https://doi.org/10.1038/s41418-019-0299-4).
- Li YL, Tian H, Jiang J, Zhang Y, Qi XW. 2020. Multifaceted regulation and functions of fatty acid desaturase 2 in human cancers. *Am J Cancer Res*. 10(12):4098–4111.
- Liang M, Ye H, Shen Q, Jiang X, Cui G, Gu W, Zhang LH, Naqvi NI, Deng YZ. 2021. Tangeretin inhibits fungal ferroptosis to suppress rice blast. *J Integr Plant Biol*. 63(12):2136–2149. doi: [10.1111/jipb.13175](https://doi.org/10.1111/jipb.13175).
- Macharia M, Das P, Naqvi N, Wong SM. 2020. iTRAQ-based quantitative proteomics reveals a ferroptosis-like programmed cell death in plants infected by a highly virulent tobacco mosaic virus mutant 24A+UPD. *Phytopathol Res*. 2(1):1. doi: [10.1186/s42483-019-0043-5](https://doi.org/10.1186/s42483-019-0043-5).
- Martin-Urdiroz M, Oses-Ruiz M, Ryder LS, Talbot NJ. 2016. Investigating the biology of plant infection by the rice blast fungus *Magnaporthe oryzae*. *Fungal Genet Biol*. 90:61–68. doi: [10.1016/j.fgb.2015.12.009](https://doi.org/10.1016/j.fgb.2015.12.009).
- Matyash V, Liebisch G, Kurzchalia TV, Shevchenko A, Schwudke D. 2008. Lipid extraction by methyl-tert-butyl ether for high-throughput lipidomics. *J Lipid Res*. 49(5):1137–1146. doi: [10.1194/jlr.D700041-JLR200](https://doi.org/10.1194/jlr.D700041-JLR200).
- McCartney AW, Dyer JM, Dhanoa PK, Kim PK, Andrews DW, McNew JA, Mullen RT. 2004. Membrane-bound fatty acid desaturases are inserted co-translationally into the ER and contain different ER retrieval motifs at their carboxy termini. *Plant Journal*. 37(2):156–173. doi: [10.1111/j.1365-313x.2004.01949.x](https://doi.org/10.1111/j.1365-313x.2004.01949.x).
- Ndiaye H, Liu JY, Hall A, Minogue S, Morgan MY, Waugh MG. 2020. Immunohistochemical staining reveals differential expression of ACSL3 and ACSL4 in hepatocellular carcinoma and hepatic gastrointestinal metastases. *Biosci Rep*. 40(4):BSR20200219. doi: [10.1042/BSR20200219](https://doi.org/10.1042/BSR20200219).
- Okuley J, Lightner J, Feldmann K, Yadav N, Lark E, Browse J. 1994. Arabidopsis FAD2 gene encodes the enzyme that is essential for polyunsaturated lipid synthesis. *Plant Cell*. 6(1):147–158. doi: [10.1105/tpc.6.1.147](https://doi.org/10.1105/tpc.6.1.147).
- Pereira SL, Leonard AE, Mukerji P. 2003. Recent advances in the study of fatty acid desaturases from animals and lower eukaryotes. *Prostaglandins Leukot Essent Fatty Acids*. 68(2):97–106. doi: [10.1016/s0952-3278\(02\)00259-4](https://doi.org/10.1016/s0952-3278(02)00259-4).
- Ryder LS, Dagdas YF, Mentlak TA, Kershaw MJ, Thornton CR, Schuster M, Chen J, Wang Z, Talbot NJ. 2013. NADPH oxidases regulate septin-mediated cytoskeletal remodeling during plant infection by the rice blast fungus. *Proc Natl Acad Sci USA*. 110(8):3179–3184. doi: [10.1073/pnas.1217470110](https://doi.org/10.1073/pnas.1217470110).
- Ryder LS, Talbot NJ. 2015. Regulation of appressorium development in pathogenic fungi. *Curr Opin Plant Biol*. 26:8–13. doi: [10.1016/j.pbi.2015.05.013](https://doi.org/10.1016/j.pbi.2015.05.013).
- Saitoh H, Fujisawa S, Mitsuoka C, Ito A, Hirabuchi A, Ikeda K, Irieda H, Yoshino K, Yoshida K, Matsumura H, et al. 2012. Large-scale gene disruption in *Magnaporthe oryzae* identifies MC69, a secreted protein required for infection by monocot and dicot fungal pathogens. *PLoS Pathog*. 8(5):e1002711. doi: [10.1371/journal.ppat.1002711](https://doi.org/10.1371/journal.ppat.1002711).
- Santomartino R, Riego-Ruiz L, Bianchi MM. 2017. Three, two, one yeast fatty acid desaturases: regulation and function. *World J Microbiol Biotechnol*. 33(5):89. doi: [10.1007/s11274-017-2257-y](https://doi.org/10.1007/s11274-017-2257-y).
- Sesma A, Osbourn AE. 2004. The rice leaf blast pathogen undergoes developmental processes typical of root-infecting fungi. *Nature*. 431(7008):582–586. doi: [10.1038/nature02880](https://doi.org/10.1038/nature02880).

- Shen Q, Liang M, Yang F, Deng YZ, Naqvi NI. 2020. Ferroptosis contributes to developmental cell death in rice blast. *New Phytol.* 227(6):1831–1846. doi: [10.1111/nph.16636](https://doi.org/10.1111/nph.16636).
- Skamnioti P, Gurr SJ. 2009. Against the grain: safeguarding rice from rice blast disease. *Trends Biotechnol.* 27(3):141–150. doi: [10.1016/j.tibtech.2008.12.002](https://doi.org/10.1016/j.tibtech.2008.12.002).
- Starikov AY, Sidorov RA, Mironov KS, Goriainov SV, Los DA. 2020. Delta or omega?  $\Delta 12$  ( $\omega 6$ ) fatty acid desaturases count 3C after the pre-existing double bond. *Biochimie.* 179:46–53. doi: [10.1016/j.biochi.2020.09.009](https://doi.org/10.1016/j.biochi.2020.09.009).
- Talbot NJ. 2003. On the trail of a cereal killer: exploring the biology of *Magnaporthe grisea*. *Annu Rev Microbiol.* 57(1):177–202. doi: [10.1146/annurev.micro.57.030502.090957](https://doi.org/10.1146/annurev.micro.57.030502.090957).
- Taylor A, Robson A, Houghton BC, Jepson CA, Ford WC, Frayne J. 2013. Epididymal specific, selenium-independent GPX5 protects cells from oxidative stress-induced lipid peroxidation and DNA mutation. *Hum Reprod.* 28(9):2332–2342. doi: [10.1093/humrep/det237](https://doi.org/10.1093/humrep/det237).
- Tomitsuka Y, Imaeda H, Ito H, Asou I, Ohbayashi M, Ishikawa F, Kuwata H, Hara S. 2023. Gene deletion of long-chain acyl-CoA synthetase 4 attenuates xenobiotic chemical-induced lung injury via the suppression of lipid peroxidation. *Redox Biol.* 66:102850. doi: [10.1016/j.redox.2023.102850](https://doi.org/10.1016/j.redox.2023.102850).
- Veneault-Fourrey C, Barooah M, Egan M, Wakley G, Talbot NJ. 2006. Autophagic fungal cell death is necessary for infection by the rice blast fungus. *Science.* 312(5773):580–583. doi: [10.1126/science.1124550](https://doi.org/10.1126/science.1124550).
- Wang X, Shen T, Lian J, Deng K, Qu C, Li E, Li G, Ren Y, Wang Z, Jiang Z, et al. 2023. Resveratrol reduces ROS-induced ferroptosis by activating SIRT3 and compensating the GSH/GPX4 pathway. *Mol Med.* 29(1):137. doi: [10.1186/s10020-023-00730-6](https://doi.org/10.1186/s10020-023-00730-6).
- Wilson RA, Talbot NJ. 2009. Under pressure: investigating the biology of plant infection by *Magnaporthe oryzae*. *Nat Rev Microbiol.* 7(3):185–195. doi: [10.1038/nrmicro2032](https://doi.org/10.1038/nrmicro2032).
- Wu J, Minikes AM, Gao M, Bian H, Li Y, Stockwell BR, Chen ZN, Jiang X. 2019. Intercellular interaction dictates cancer cell ferroptosis via NF2-YAP signalling. *Nature.* 572(7769):402–406. doi: [10.1038/s41586-019-1426-6](https://doi.org/10.1038/s41586-019-1426-6).
- Xiao R, Zou Y, Guo X, Li H, Lu H. 2022. Fatty acid desaturases (FADs) modulate multiple lipid metabolism pathways to improve plant resistance. *Mol Biol Rep.* 49(10):9997–10011. doi: [10.1007/s11033-022-07568-x](https://doi.org/10.1007/s11033-022-07568-x).
- Xuan Y, Wang H, Yung MM, Chen F, Chan WS, Chan YS, Tsui SK, Ngan HY, Chan KK, Chan DW. 2022. SCD1/FADS2 fatty acid desaturases equipose lipid metabolic activity and redox-driven ferroptosis in ascites-derived ovarian cancer cells. *Theranostics.* 12(7):3534–3552. doi: [10.7150/thno.70194](https://doi.org/10.7150/thno.70194).
- Yamane D, Hayashi Y, Matsumoto M, Nakanishi H, Imagawa H, Kohara M, Lemon SM, Ichi I. 2022. FADS2-dependent fatty acid desaturation dictates cellular sensitivity to ferroptosis and permissiveness for hepatitis C virus replication. *Cell Chem Biol.* 29(5):799–810. doi: [10.1016/j.chembiol.2021.07.022](https://doi.org/10.1016/j.chembiol.2021.07.022).
- Yan X, Talbot NJ. 2016. Investigating the cell biology of plant infection by the rice blast fungus *Magnaporthe oryzae*. *Curr Opin Microbiol.* 34:147–153. doi: [10.1016/j.mib.2016.10.001](https://doi.org/10.1016/j.mib.2016.10.001).
- Yang F, Xiao Y, Ding JH, Jin X, Ma D, Li DQ, Shi JX, Huang W, Wang YP, Jiang YZ, et al. 2023. Ferroptosis heterogeneity in triple-negative breast cancer reveals an innovative immunotherapy combination strategy. *Cell Metab.* 35(1):84–100. doi: [10.1016/j.cmet.2022.09.021](https://doi.org/10.1016/j.cmet.2022.09.021).
- Yang L, Cao LM, Zhang XJ, Chu B. 2022. Targeting ferroptosis as a vulnerability in pulmonary diseases. *Cell Death Disease.* 13(7):649. doi: [10.1038/s41419-022-05070-7](https://doi.org/10.1038/s41419-022-05070-7).
- Yang WS, Stockwell BR. 2016. Ferroptosis: death by lipid peroxidation. *Trends Cell Biol.* 26(3):165–176. doi: [10.1016/j.tcb.2015.10.014](https://doi.org/10.1016/j.tcb.2015.10.014).
- Zhang L, Zhang D, Chen Y, Ye W, Lin Q, Lu G, Ebbole DJ, Olsson S, Wang Z. 2019. *Magnaporthe oryzae* CK2 accumulates in nuclei, nucleoli, at septal pores and forms a large ring structure in appressoria, and is involved in rice blast pathogenesis. *Front Cell Infect Microbiol.* 9:113. doi: [10.3389/fcimb.2019.00113](https://doi.org/10.3389/fcimb.2019.00113).
- Zhao S, Sun J, Sun J, Zhang X, Zhao C, Pan J, Hou L, Tian R, Wang X. 2022. Insights into the novel FAD2 gene regulating oleic acid accumulation in peanut seeds with different maturity. *Genes.* 13(11):2076. doi: [10.3390/genes13112076](https://doi.org/10.3390/genes13112076).